HHS Public Access

Author manuscript

Magn Reson Med. Author manuscript; available in PMC 2016 October 01.

Published in final edited form as:

Magn Reson Med. 2015 October ; 74(4): 1032–1041. doi:10.1002/mrm.25495.

Free-breathing Combined 3D Phase Sensitive Late Gadolinium Enhancement and T_1 Mapping for Myocardial Tissue Characterization

Sebastian Weingärtner[1,2], **Mehmet Akçakaya**[1], **Sébastien Roujol**[1], **Tamer Basha**[1], **Cory Tschabrunn**[1], **Sophie Berg**[1], **Elad Anter**[1], and **Reza Nezafat**[1]

[1]Department of Medicine, Beth Israel Deaconess Medical Center and Harvard Medical School, Boston, MA

[2]Computer Assisted Clinical Medicine, University Medical Center Mannheim, Heidelberg University, Mannheim, Germany

Abstract

Purpose—To develop a novel MR sequence for combined 3D phase-sensitive (PS) late gadolinium enhancement (LGE) and T_1 mapping to allow for simultaneous assessment of focal and diffuse myocardial fibrosis.

Methods—In the proposed sequence, four 3D imaging volumes are acquired with different T_1 weightings using a combined saturation and inversion preparation, after administration of a gadolinium contrast agent. One image is acquired fully sampled with the inversion time selected to null the healthy myocardial signal (the LGE image). The other three images are three-fold under-sampled and reconstructed using compressed sensing. An acquisition scheme with two interleaved imaging cycles and joint navigator-gating of those cycles ensures spatial registration of the imaging volumes. T_1 maps are generated using all four imaging volumes. The signal-polarity in the LGE image is restored using supplementary information from the T_1 fit to generate PS-LGE images. The accuracy of the proposed method was assessed with respect to a inversion-recovery spin-echo sequence. In-vivo T_1 maps and LGE images were acquired with the proposed sequence and quantitatively compared to 2D multi-slice Modified Look-Locker inversion recovery (MOLLI) T_1 maps. Exemplary images in a patient with focal scar were compared to conventional LGE imaging.

Results—The deviation of the proposed method and the spin-echo reference was < 11 ms in phantom for T_1 times between 250 and 600 ms, regardless of the inversion time selected in the LGE image. There was no significant difference in the in-vivo T_1 times of the proposed sequence and the 2D MOLLI technique (myocardium: 292 ± 75 ms vs. 310 ± 49 ms, blood-pools: 191 ± 75 ms vs. 182.0 ± 33). The LGE images showed proper nulling of the healthy myocardium in all subjects and clear depiction of scar in the patient.

Conclusion—The proposed sequence enables simultaneous acquisition of 3D PS-LGE images and spatially registered 3D T_1 maps in a single scan.

Correspondence to:, Reza Nezafat, Ph.D., Beth Israel Deaconess Medical Center, 330 Brookline Ave, Boston, MA, 02215, Phone: 617-667-1747 ; Fax: 617-975-5480, rnezafat@bidmc.harvard.edu.

Keywords

myocardial T_1 mapping; diffused fibrosis; LGE imaging; 3D imaging; compressed sensing; quantitative cardiac MRI; phase sensitive imaging

Introduction

Late gadolinium enhancement (LGE) MRI using an inversion recovery based sequence is clinically established for depiction of left ventricular (LV) scar (1,2). In this sequence, the k-space data are acquired after an inversion pulse. The inversion time delay (TI) is chosen to null signal from healthy myocardium, thereby creating contrast between healthy myocardium, blood and scarred myocardium (3). The optimal TI time is commonly selected by performing a Look-Locker sequence prior to the LGE scan (4). The phase-sensitive inversion recovery sequence (PSIR) was introduced over a decade ago to reduce the sensitivity of LGE imaging to an incorrect choice of TI (5). With PSIR, the LGE image acquisition is interleaved with the acquisition of a phase map, which enables polarity restoration in the magnitude data for the trade-off against increased scan-time.

Clinically, LGE images are visually assessed for the presence and pattern/location focal or diffuse hyper-enhancement (6). Different myocardial diseases result in different patterns of hyper-enhancement. Patients with myocardial infarction usually exhibit subendocardial enhancement (3,7,8). Non-ischemic cardiomyopathy patients usually have a mid-myocardial or epicardial based hyper-enhancement (9,10). Patients with hypertrophic cardiomyopathy show hyper-enhancement in the insertion areas of the right ventricle with “patchy” signal enhancement (11–13). The extent of the scar can be quantified, which adds additional prognostic value beyond qualitative assessment (14–18). Beyond assessment of the scar extent, the prognostic value of the area of the infarct border zone, i.e. region with intermediate signal intensity, for adverse cardiac events has been widely investigated (19–21). While LGE can detect focal fibrosis, it is not able to provide information about the presence and amount of the diffuse fibrosis in the myocardium.

Post-contrast myocardial T_1 mapping sequences have been recently used for evaluation of diffuse myocardial fibrosis (22,23). In this technique, the T_1 relaxation time is measured quantitatively after injection of an extracellular contrast-agent. In patients with focal myocardial fibrosis such as patients with prior myocardial infarction, there is an accumulation of the exogenous contrast agent in the area of focal fibrosis, which results in reduced T_1 values (24). Furthermore, in regions with evidence of diffuse myocardial fibrosis, post-contrast T_1 relaxation time is reduced as well (23).

To assess for both focal and diffuse fibrosis, LGE and T_1 mapping data are usually acquired in two separate scans with multiple separate breath-holds. For complete coverage of LV, LGE scans are usually performed with 10–12 short-axis views. However, T_1 mapping is commonly acquired in 1 to 3 slices. This limits our ability to simultaneously assess for both focal and diffuse fibrosis. Although, additional scans can be performed to provide full LV coverage for T_1 maps, it will significantly increase the number of breath-holds and may result in mis-registration of datasets acquired in separate breath-holds. Therefore, a

combined LGE/T_1 mapping sequence with full LV coverage may improve our ability to more fully characterize myocardial tissue composition.

In this study, we propose a novel combined LGE and T_1 mapping sequence with volumetric LV coverage, which also enables phase sensitive (PS) LGE imaging. This combined sequence allows for the simultaneous assessment of both focal and diffuse fibrosis during free-breathing. Phantom and in vivo experiments were performed to evaluate the proposed sequence.

Methods

Sequence

Figure 1 shows the proposed sequence that combines a 3D phase sensitive LGE scan with 3D T_1 mapping (PS-LGE/T_1). Four 3D saturation pulse prepared inversion recovery imaging volumes with different inversion times T_{inv}^{null}, T_{inv}^{1}, T_{inv}^{2}, and T_{inv}^{3} are acquired. Out of four inversion times, one T_{inv}^{null} is chosen to null the healthy myocardium, analogous to a conventional LGE sequence. We refer to this volume as the LGE volume. The other 3 inversion times (T_{inv}^{1}, T_{inv}^{2}, and T_{inv}^{3}) are linearly distributed between the minimal and maximal applicable inversion time range and we refer to these 3 images as supplementary imaging volumes. A saturation pulse is applied immediately after the R-wave of the ECG to erase the magnetization history and remove susceptibilities to incomplete longitudinal magnetization recovery, as previously shown in SAturation Pulse Prepared Heart-rate independent Inversion REcovery (SAPPHIRE) sequence (25).

We performed the acquisition of the four imaging volumes in two interleaved acquisition cycles (referred to as interleaves). The first interleaf is always used to collect LGE imaging data. The data acquisition in the second interleaf cycles through the three different inversion times of the supplementary imaging volumes. The order of the supplementary inversion times is randomly permutated. The proposed scheme leads to full sampling of the LGE data while the supplementary images are acquired with an undersampling factor of three. An exemplary sampling pattern of the proposed sequences is shown in Figure 3.

The k-space lines are acquired in a pseudo-radial view order, i.e. the Cartesian k-space lines acquired per heart-cycle form a pseudo radial spoke in the k_y−k_z plane (26). Acquiring a random subset of these spokes results in a pseudo-random undersampling pattern. To allow full sampling of the central k-space for all three supplementary T_1-weighted images and the LGE image, the central k-space segments are acquired separately and non-interleaved for each imaging volume at the beginning of the scan. This scheme results in a fully sampled LGE image and three undersampled supplementary images with pseudo-random undersampling in the outer k-space and a fully sampled k-space center. Hence, the supplementary images are suited for reconstruction using a compressed sensing algorithm (27,28). The size of the k-space center that allows robust reconstructions is chosen relative to the k-space matrix size, as explained in the imaging parameters below.

Respiratory Motion

To enable voxel-wise estimation of the T_1 values, all four volumes need to be spatially aligned. Respiratory-induced motion can severely impact this alignment, as well as the effective resolution and accuracy of the T_1 maps (29,30). Hence, for the area outside the fully sampled k-space center ("outer k-space"), which is necessary for a robust compressed sensing reconstruction, we used a joint navigator (NAV)-gating to minimize inter-volume mis-registration (31,32). In the proposed scheme data are only accepted if the NAV-signal of two consecutive interleaves (starting either with an LGE interleaf or with a supplementary interleaf) is within the predefined gating window.

The proposed sequence was implemented using a spiral-beam navigator, positioned at the dome of the right hemi-diaphragm for in-vivo measurements. Spatially selective re-inversion was performed right after the inversion-pulse of the magnetization preparation. The gating window for the joint gating scheme was set to 7 mm. Furthermore, prospective slice-tracking with a fixed tracking factor of 0.6 was used.

Reconstruction

Figure 2 illustrates the reconstruction scheme, which is employed to generate the 3D LGE image and the 3D T_1 map from the four imaging volumes. The LGE volume is reconstructed from the fully sampled data using 3D Fast Fourier Transform. The three undersampled supplementary T_1-weighted volumes are reconstructed using Low-dimensional-structure self-learning and thresholding (LOST) (33,34). T_1 maps are generated by performing a voxel-wise curve fitting to the image intensities of all four T_1-weighted imaging volumes. The following model was derived from the Bloch equations, for the case of the combined saturation and inversion recovery under the assumption of perfect inversion efficiency

$$S(M_0, T_1) = M_0(1 - (2 - e^{-(T_{sat} - T_{inv})/T_1})e^{-T_{inv}/T_1}), \quad [1]$$

where M_0 is the spin density and T_1 the longitudinal relaxation time. The timing variables T_{sat} and T_{inv} are defined as shown in Figure 1.

The signal-polarity for the T_1 fit is restored as described in (22): The images are sorted based on the inversion time in ascending order. A first curve-fit is performed on the data, where all intensities are assumed to be positive. A second curve-fit is performed with data, where a negative sign is assigned only to the image with the shortest inversion time and so on. The curve-fit that results in the least residual is assumed to generate the right polarity restoration.

In the fit process the signal-polarity is restored for all imaging volumes, including the LGE image. As proposed in the PSIR technique (5), a polarity-restored LGE image provides increased robustness to inaccurate TI. Therefore, we propose to use the information obtained in the T_1 fit process to obtain a polarity-restored LGE image with increased contrast between healthy normal myocardium and scar. For this purpose, we apply the signal-polarity of the T_1 fit voxel-wise to the magnitude LGE image. If, for any given voxel, the data point with the inversion time T_{inv}^{null} was assigned with a negative sign in the fit with the least

residual, then the image intensity in this voxel of the polarity-restored LGE image is the negative of the intensity in the magnitude LGE image. In all the other voxels, the polarity-restored LGE image and the magnitude LGE image are identical.

Phantom Imaging

All phantom studies were performed on a 1.5T Philips Achieva (Philips, Best, The Netherlands) system using a 32 channel cardiac coil array. The phantom consisted of 4 vials containing $NiCl_2$ doped agarose-gel with varying concentrations, resulting in T_1 times between 250 and 600 ms.

The phantom was imaged using the proposed PS-LGE/T_1 sequence and an inversion recovery spin-echo sequence as reference. The PS-LGE/T_1 sequence was performed multiple times, with the inversion time of the LGE image volume adjusted to null different vials. The proposed sequence was performed with a spoiled gradient echo imaging readout (FOV = 320×320×100 mm^3, resolution = 1.5×1.5×10 mm^3, TR/TE = 5.2 ms/2.6 ms, flip angle = 25°, readout band-width=289 Hz per pixel, 5 startup pulses). Ten repetitions were performed for each LGE/T_1 sequence to assess the reproducibility in phantom. All scans were performed using a simulated electrocardiogram (ECG) with a heart rate of 60 bpm.

For reference a 2D inversion-recovery spin-echo sequence was performed using the following parameters: TR/TE = 15 s/10 ms, flip angle = 90°, resolution = 1.3 × 1.3 mm^2, slice-thickness = 5 mm, 17 inversion times logarithmically spaced between 50 and 3000 ms, scan time = 6 hours. The slice position of the spin-echo sequence was spatially aligned with the central slice of the PS-LGE/T_1 acquisition.

The accuracy of the studied sequences was assessed as the absolute deviation between the spin-echo reference and the average T_1 times in a manually drawn region of interest (ROI), averaged over all repetitions.

In-vivo Imaging

The study was approved by the institutional review board and written informed consent was acquired prior to each examination. All in-vivo imaging was performed on a 1.5T Philips Achieva (Philips, Best, The Netherlands) system using a 32 channel cardiac coil array. Ten healthy adult subjects (4 male, 34±16 years) and one patient (male, 54 years old) with hypertrophic cardiomyopathy (HCM) were imaged. All subjects were imaged after intravenous administration of 0.2 mmol/kg gadobenate dimeglumine (MultiHance, Bracco SpA, Milano, Italy).

All healthy subjects were imaged with the proposed PS-LGE/T_1 sequence and multi-slice 2D MOLLI for comparison of the acquired T_1 maps. The acquisition time after contrast 17 ± 9 minutes (8 – 31 minutes) for the PS-LGE/T_1 sequence and 18 ± 10 minutes (7 – 38 minutes) for MOLLI. The HCM patient was imaged using the proposed PS-LGE/T_1 sequence 13 minutes after contrast injection and with conventional LGE imaging 25 minutes after contrast injection. The patient was in sinus-rhythm with scattered premature beats, during the MRI scan.

To further demonstrate the feasibility of PS-LGE/T1 sequence in imaging scar, we added our imaging sequence to an imaging protocol of swine models with prior myocardial infarctions. A closed-chest myocardial infarction was performed in the Beth Israel Deaconess Medical Center experimental electrophysiology laboratory and conformed to the position of the American Heart Association on Research Animal Use as well as the Declaration of Helsinki. The protocol was approved by the institutional animal care and use committee. Three male Yorkshire swine weighing 33–35 kg were pre-medicated for 3–5 days with oral amiodarone (800mg BID), preanesthetized with telazol (5.7 mg/kg IM), and then anesthetized with inhaled isoflurane during the procedure. The animals were intubated and ventilation was maintained between 10 and 16 breaths/min with tidal volumes between 300–500 mL. Percutaneous balloon occlusion of the mid-left anterior descending coronary artery (LAD) immediately distal to the second diagonal branch was performed for 180 minutes using a 2.5×12 mm angioplasty balloon via a retrograde aortic approach. The imaging was performed 4–5 weeks after the procedure. Imaging was performed with the proposed sequence approximately 30 minutes after contrast injection of .2 mmol/kg gadobenate dimeglumine. The animal had a heart-rate of 95 bpm during the imaging.

The proposed PS-LGE/T_1 sequence was performed with a spoiled gradient echo imaging readout and the following sequence parameters: FOV = 320×320×100 mm^2, TR/TE = 5.2 ms/2.6 ms, flip angle = 25°, band-width = 289 Hz/Px, 5 startup pulses. The resolution was 1.5×1.5×4 mm^3 for 4 subjects, 1.5×1.5×7 mm^3 for one subject, and 1.5×1.5×10 mm^3 for 3 subjects and the animal study. A subject-specific acquisition window length was chosen to fit in the end-diastolic quiescent period, as obtained from a cine scout image at the beginning of the scan. The center size was chosen to cover 15% along the k_y and 25% along k_z for all undersampled k-space matrices. Conventional LGE imaging was performed using inversion recovery prepared spoiled-gradient echo imaging with the same imaging parameters as the proposed LGE/T_1 sequence. The inversion times for nulling of the healthy normal myocardial signal in the proposed LGE/T_1 and the conventional LGE sequence were determined using Look-Locker scouts. MOLLI T_1 mapping was performed with FOV = 320×320 mm^2, in-plane resolution = 1.7×2.1 mm^2, slice-thickness = 10 mm, TR/TE = 2.6 ms/1.0 ms, flip angle = 40°, SENSE rate = 2, 3 – 10 slices. The nominal scan time was 5:20 minutes for the proposed PS-LGE/T_1 (20 seconds k-space center / 5:00 minutes outer k-space), 2:40 minutes for conventional LGE imaging and 2:40 minutes for MOLLI (with 10 slices) assuming 100% gating efficiency at 60 beats per minute and no rest periods between the breath holds.

The mean and standard deviation of the T_1 values in the myocardium, and the left and right ventricular blood pools were measured by manually drawing regions of interest. The ROI for the myocardium was drawn to cover the entire LV. The T_1 times were compared between the proposed sequence and MOLLI using the paired student's t-test. A p-value of <0.05 was considered to be significant. Additionally, T_1 times in the healthy myocardium, the core scar region and the surrounding heterogeneous tissue were assessed in the HCM patient using manually drawn ROIs in the T_1 maps generated with the proposed sequence.

Results

Phantom Imaging

Table 1 shows the results of T_1 measurements with the proposed PS-LGE/T_1 sequence compared to the spin-echo reference in the phantom. The proposed sequence is in close agreement with the spin-echo reference for T_1 times in the post-contrast range. The deviations from the spin-echo sequence were less than 11 ms (< 2%). No systematic impairment of the accuracy was observed for varying inversion times in the LGE image.

In-Vivo Imaging

Figure 4 shows representative slices of 3D LGE images and 3D T_1 maps acquired with the proposed sequence in a healthy adult subject. The LGE images provide good contrast between the myocardium and the ventricular blood-pools, and show robust nulling of the healthy myocardial tissue. The T_1 maps are compared to maps acquired with a 2D multi-slice MOLLI sequence. Figure 5 depicts the T_1 times estimated with the proposed sequence and 2D MOLLI in the LV and the LV and RV blood pools, on a subject-by-subject basis, as well as Bland-Altman plots comparing the two sequences. The quantitative analysis of the T_1 times showed no significant difference of the average T_1 times in the myocardium or the blood pools between MOLLI and the proposed technique (Myocardium: 292 ± 75 ms LGE/T1, 310 ± 49 ms MOLLI, $p > 0.3$; blood-pools: 191 ± 76 ms LGE/ T_1, 182 ± 33 ms MOLLI, $p > 0.3$). In terms of precision, as measured by the signal homogeneity, the proposed technique is less precise than MOLLI in the myocardium, although the difference is not significant (106 ± 72 ms vs. 63 ± 14 ms for the proposed technique and MOLLI respectively, $p = 0.16$). The proposed technique provides a significant improvement in terms of the homogeneity in the blood pool (12 ± 7 ms vs. 25 ± 8 ms for the proposed technique and MOLLI respectively, $p < 0.01$). Bland-Altman analysis shows no systematic variations, although more pronounced differences are observed for lower T_1 values. The average scan time of the proposed sequence was 14:46 min with a gating efficiency of 43% ± 16% (range: 23% – 74%).

Figure 6 shows a representative example illustrating the polarity restoration with the proposed sequence. The top row depicts four inversion recovery imaging volumes after reconstruction. The magnitude intensity for a single voxel is shown in the second row. Successively assigning negative signs, to the data points, results in five data sets, which are fitted to the relaxation model. Only the one with the least residual is assumed to restore the polarity correctly. The signs from the corresponding least-residual fit are multiplied voxel-wise with the magnitude of the original imaging volumes, resulting in the signed imaging volumes, as shown in the bottom row.

Figure 7 shows example slices of a LGE image with an imperfect inversion time choice acquired with the proposed sequence and reconstructed without signal polarity restoration in a healthy subject, which results in residual signal and incomplete nulling of the myocardium is observed. Nulling of the healthy myocardium can be readily seen in the images after polarity restoration.

Figure 8 shows LGE images and T_1 maps acquired with a conventional 3D LGE sequence and the proposed PS-LGE/T_1 sequence in the HCM patient. As indicated by the arrows, clear depiction of scar at the RV insertion is achieved with both sequences. Clear depiction of the scar is also observed in the 3D T_1 maps as shown in the lowest row of Figure 8. The quantitatively assessed post-contrast T_1 time was 317 ± 37 ms in a ROI in the healthy myocardium as measured in a remote area of the lateral wall, 126 ± 7 ms in the core area of the scar and 171 ± 5 ms in the scar border zone. Figure 9 shows the results from the animal study. Large left ventricular scar is clearly depicted in the LGE images (arrows). Furthermore, the scar areas show substantially decreased T_1 times in the T_1 maps acquired with the proposed sequence.

Discussion

In this study we demonstrated a novel pulse sequence for the simultaneous acquisition of 3D PS-LGE and T_1 maps by acquiring four inversion recovery images, in which one is acquired with an inversion time that nulls the healthy myocardium. The LGE image is reconstructed from the fully-sampled data-set using simple Fourier transform. The T_1 map is generated using voxel-wise curve fitting of the four imaging datasets acquired with different inversion times. To improve image quality of LGE, the LGE data was acquired fully-sampled, but the other three data-sets were acquired with an undersampling factor of 3 with fully-sampled center of k-space and undersampled outer k-space. These undersampled data sets are reconstructed using compressed-sensing prior to curve fitting for estimating T_1 values. A joint navigator-gating scheme was used to improve alignment of the four datasets. Furthermore, the information from the recovery curve of T_1 is used to generate polarity-restored LGE images similar to the PSIR sequence.

The proposed 3D PS-LGE/T_1 method is different than the conventional PSIR LGE and MOLLI T_1 mapping in several respects. Conventional PSIR LGE acquires two imaging volumes in alternating heartbeats to enable polarity restoration. The proposed method, on the other hand, uses the acquisition during the alternating heartbeat to cycle through three additional undersampled images, which are used both for polarity restoration and T_1 mapping, without increasing the scan time when compared to PSIR LGE. When compared to multi-slice 2D MOLLI T_1 mapping, the proposed method offers volumetric coverage, robustness to slice mis-registration, higher baseline SNR, which was used for improved spatial resolution, as well as a shorter segmented acquisition window which may reduce the effects of cardiac motion. Furthermore, the magnetization preparation used in the proposed technique allows heart-rate independence and arrhythmia robustness (25) for both LGE imaging and T_1 mapping. This is achieved by applying a saturation pulse immediately after each R-wave, erasing the magnetization history, as previously proposed for LGE imaging in patients with arrhythmia (25).

The proposed acquisition scheme in two interleaved acquisition cycles with a fully sampled LGE image requires a trade-off between the number of supplementary images and the undersampling factor. For the applied matrix-size and k-space center size in this study, a 3-fold acceleration resulted in robust reconstructions with the LOST reconstruction, based on subjective visual assessment. However, if the sequence is applied with smaller matrix-sizes,

lower undersampling factors might be necessary, allowing only a reduced number of supplementary images.

A random undersampling pattern is required to enable the use of compressed-sensing reconstructions of the supplementary data. For this purpose a pseudo radial k-space ordering (the k-space lines acquired per heart-cycle resemble a pseudo radial spoke in the k_y–k_z plane) is employed and the order of the supplementary inversion times is randomly permutated during the scan. A random subset of the spokes resulted in random undersampling of the k-space and enabled artifact-free compressed sensing reconstructions.

The precision in a T_1 map, assessed as the standard deviation in a homogenous area, is typically used as a surrogate for the noise-resilience and the fit-conditioning of a T_1 mapping method. However, compressed sensing reconstructions, involve spatial regularization and smoothing of the image intensities. This can lead to filtering effects that artificially increase the precision and limit the use of this metric for the assessment of noise-resilience in the T_1 maps. However, the standard deviation in an area with homogenous T_1 also reflects the presence of motion artifacts, outlying T_1 times due to failed curve-fitting and partial voluming. The low standard deviation reported with the proposed method indicates robustness to these factors, which potential eases the clinical assessment of myocardial T_1 times.

T_1 maps generated with the proposed 3D PS-LGE/T1 sequence have increased T_1 values in the inferior/lateral wall. We hypothesize that this inhomogeneity may be related to the choice of the phase encoding direction, which was in the foot-head direction for these acquisitions. Thus, any residual aliasing artifacts or motion artifacts would be apparent in this direction. While, these were not readily visualized in the individual reconstructed images, their effect may be significant enough to affect the fitting process and causing inhomogeneities in the T_1 maps. We note that a similar inhomogeneity is apparent in the MOLLI maps in the anterior-posterior direction, which was used as the phase encoding direction for these 2D images. For the lower myocardial T_1 values, there is a more pronounced variability between the two T_1 mapping methods. As these differences were not observed in phantom imaging, these may be due to changes in the contrast wash-out in between the acquisition of the two sequences.

The proposed sequence was implemented with a joint navigator gating of two acquisition cycles, resulting in an average gating efficiency of 43%. However, the navigator efficiency of the proposed scheme was highly subject-dependent. Specifically, it depends on the ratio of the heart-rate to the respiratory cycle length. Long respiratory cycle lengths or high heart-rates lead to small reductions in the navigator efficiency of the joint navigator gating compared to conventional navigator, while very low heart-rates with a fast breathing pattern result in a bad acceptance rate and long scan times.

Most recent T_1 mapping methods employ a bSSFP imaging readout (35). However, to obtain conventional, T_1 weighted contrast for the LGE image (6), a GRE imaging readout was used in the proposed sequence. Repeated GRE excitations can cause strong perturbations of the longitudinal magnetization recovery curve, potentially impairing the

quantitative assessment of the T1 time. However, in the proposed sequence a central k-space ordering was used. Therewith, the longitudinal magnetization is only perturbed by the startup pulses before the central k-space is acquired, enabling T1 mapping with high-accuracy in the post-contrast regime with the proposed method, despite the use of GRE.

As in previously reported methods for 3D T_1 mapping (36,37) the number of sample points along the T_1 recovery curve is lower than in conventional 2D methods. The acquired T_1 maps are still of high precision, as the individual T_1 weighted images have improved SNR compared to 2D acquisitions. However, fewer sampling points increase the susceptibility of the accuracy of the T_1 mapping method to the choice of the inversion times. In the current study, we did not perform any optimization for the inversion times. An analysis of the optimal sampling times to increase robustness and accuracy of the proposed T_1 estimation (38) is warranted. Also, due to the low number of sampling points, a two-parameter model, with the assumption of perfect inversion, was employed. Especially in the presence of major field inhomogeneities or susceptibility artifacts this can lead to decreased accuracy of the T1 estimation in-vivo.

Only a single patient with scar in the myocardium was imaged in the present study. However, a number of detrimental factors, including irregular cardiac and respiratory motion, is known to lead to inferior image quality in patients compared to healthy subjects with commonly used T_1 mapping techniques. The proposed method employs the SAPPHIRE magnetization preparation. This was previously shown to provide robust T_1 weighted image contrast regardless of the cardiac rhythm, eliminating the susceptibility of the imaging contrast to heart rate regularity. Furthermore, unlike in single-shot myocardial T_1 mapping methods, the acquisition window was adapted to the individual duration of the diastolic quiescent periods to minimize imaging artifacts caused by cardiac motion. In the presence of substantial arrhythmias, a joint rejection of the two interleaves based on arrhythmia detection can be used to further reduce the influence of cardiac motion for the trade-off of increased scan time. More irregular or fast breathing pattern in patients might lead to longer scan times than in healthy subjects. Increased gating window sizes in combination with retrospective image registrations, as recently developed for cardiac T_1 mapping applications could be employed for mitigating this problem. Further studies in patients with focal or diffuse fibrosis in the presence of irregular cardiac or respiratory motion are needed to clinically validate the imaging sequence.

Our study has several limitations. We did not systematically study different undersampling rates but arbitrary chose an acceleration rate of 3 for T_1 mapping datasets. Although there are several alternative T_1 imaging sequences such as SASHA (39), ShMOLLI (40), SAPPHIRE (25) or SAP-T1 (41) we only compared T_1 values with those acquired with MOLLI sequence. Further studies are warranted to study the reproducibility of the proposed technique in vivo.

Conclusion

We present a novel pulse sequence for simultaneous free-breathing 3D LGE and T_1 mapping that enables assessment of focal and diffuse fibrosis in a single scan. This sequence provides

T_1 measurements similar to the conventional 2D T_1 maps of MOLLI, and LGE images with restored polarity.

Acknowledgements

The authors thank Warren J. Manning for editing this paper. S.W. acknowledges financial support from the Deutsche Telekom Stiftung.

The project described was supported by NIH R01EB008743-01A2. Sebastian Weingärtner is supported by a fellowship from the Deutsche Telekom Stiftung.

References

1. Kim RJ, Fieno DS, Parrish TB, Harris K, Chen E-L, Simonetti O, Bundy J, Finn JP, Klocke FJ, Judd RM. Relationship of MRI delayed contrast enhancement to irreversible injury, infarct age, contractile function. Circulation. 1999; 100(19):1992–2002. [PubMed: 10556226]
2. Kim RJ, Wu E, Rafael A, Chen E-L, Parker MA, Simonetti O, Klocke FJ, Bonow RO, Judd RM. The use of contrast-enhanced magnetic resonance imaging to identify reversible myocardial dysfunction. N Engl J Med. 2000; 343(20):1445–1453. [PubMed: 11078769]
3. Simonetti OP, Kim RJ, Fieno DS, Hillenbrand HB, Wu E, Bundy JM, Finn JP, Judd RM. An improved MR imaging technique for the visualization of myocardial infarction. Radiology. 2001; 218(1):215–223. [PubMed: 11152805]
4. Look DC, Locker DR. Time saving in measurement of NMR and EPR relaxation times. Review of Scientific Instruments. 1970; 41(2):250–251.
5. Kellman P, Arai AE, McVeigh ER, Aletras AH. Phase-sensitive inversion recovery for detecting myocardial infarction using gadolinium-delayed hyperenhancement†. Magn Reson Med. 2002; 47(2):372–383. [PubMed: 11810682]
6. Kim RJ, Shah DJ, Judd RM. How we perform delayed enhancement imaging. J Cardiovasc Magn Reson. 2003; 5(3):505–514. [PubMed: 12882082]
7. Wu E, Judd RM, Vargas JD, Klocke FJ, Bonow RO, Kim RJ. Visualisation of presence, location, and transmural extent of healed Q-wave and non-Q-wave myocardial infarction. Lancet. 2001; 357(9249):21–28. [PubMed: 11197356]
8. Selvanayagam JB, Kardos A, Francis JM, Wiesmann F, Petersen SE, Taggart DP, Neubauer S. Value of delayed-enhancement cardiovascular magnetic resonance imaging in predicting myocardial viability after surgical revascularization. Circulation. 2004; 110(12):1535–1541. [PubMed: 15353496]
9. Shehata ML, Turkbey EB, Vogel-Claussen J, Bluemke DA. Role of cardiac magnetic resonance imaging in assessment of nonischemic cardiomyopathies. Top Magn Reson Imaging. 2008; 19(1): 43–57. [PubMed: 18690160]
10. Bluemke DA. MRI of nonischemic cardiomyopathy. Am J Roentgenol. 2010; 195(4):935–940. [PubMed: 20858821]
11. Teraoka K, Hirano M, Ookubo H, Sasaki K, Katsuyama H, Amino M, Abe Y, Yamashina A. Delayed contrast enhancement of MRI in hypertrophic cardiomyopathy. Magen Reson Imag. 2004; 22(2):155–161.
12. Wilson JM, Villareal RP, Hariharan R, Massumi A, Muthupillai R, Flamm SD. Magnetic resonance imaging of myocardial fibrosis in hypertrophic cardiomyopathy. Tex Heart I J. 2002; 29(3):176–180.
13. Bogaert J, Goldstein M, Tannouri F, Golzarian J, Dymarkowski S. Late myocardial enhancement in hypertrophic cardiomyopathy with contrast-enhanced MR imaging. Am J Roentgenol. 2003; 180(4):981–985. [PubMed: 12646440]
14. Moon J, Hong YJ, Kim YJ, Shim CY, Jang Y, Chung N, Cho SY, Ha JW. Extent of late gadolinium enhancement on cardiovascular magnetic resonance imaging and its relation to left ventricular longitudinal functional reserve during exercise in patients with hypertrophic cardiomyopathy. Circ J. 2013; 77(7):1742–1749. [PubMed: 23546472]

15. Fluechter S, Kuschyk J, Wolpert C, Doesch C, Veltmann C, Haghi D, Schoenberg SO, Sueselbeck T, Germans T, Streitner F, Borggrefe M, Papavassiliu T. Extent of late gadolinium enhancement detected by cardiovascular magnetic resonance correlates with the inducibility of ventricular tachyarrhythmia in hypertrophic cardiomyopathy. J Cardiovasc Magn Reson. 2010; 12:30. [PubMed: 20492668]
16. Alexandre J, Saloux E, Dugue AE, Lebon A, Lemaitre A, Roule V, Labombarda F, Provost N, Gomes S, Scanu P, Milliez P. Scar extent evaluated by late gadolinium enhancement CMR: a powerful predictor of long term appropriate ICD therapy in patients with coronary artery disease. J Cardiovasc Magn Reson. 2013; 15:12. [PubMed: 23331500]
17. Kwon DH, Halley CM, Carrigan TP, Zysek V, Popovic ZB, Setser R, Schoenhagen P, Starling RC, Flamm SD, Desai MY. Extent of left ventricular scar predicts outcomes in ischemic cardiomyopathy patients with significantly reduced systolic function: a delayed hyperenhancement cardiac magnetic resonance study. JACC Cardiovasc Imaging. 2009; 2(1):34–44. [PubMed: 19356530]
18. Srichai MB, Schvartzman PR, Sturm B, Kasper JM, Lieber ML, White RD. Extent of myocardial scarring on nonstress delayed-contrast-enhancement cardiac magnetic resonance imaging correlates directly with degrees of resting regional dysfunction in chronic ischemic heart disease. Am Heart J. 2004; 148(2):342–348. [PubMed: 15309007]
19. Yan AT, Shayne AJ, Brown KA, Gupta SN, Chan CW, Luu TM, Di Carli MF, Reynolds HG, Stevenson WG, Kwong RY. Characterization of the peri-Infarct zone by contrast-enhanced cardiac magnetic resonance imaging is a powerful predictor of post–myocardial infarction mortality. Circulation. 2006; 114(1):32–39. [PubMed: 16801462]
20. Schmidt A, Azevedo CF, Cheng A, Gupta SN, Bluemke DA, Foo TK, Gerstenblith G, Weiss RG, Marbán E, Tomaselli GF, Lima JAC, Wu KC. Infarct tissue heterogeneity by magnetic resonance imaging identifies enhanced cardiac arrhythmia susceptibility in patients with left ventricular dysfunction. Circulation. 2007; 115(15):2006–2014. [PubMed: 17389270]
21. Rayatzadeh H, Tan A, Chan RH, Patel SJ, Hauser TH, Ngo L, Shaw JL, Hong SN, Zimetbaum P, Buxton AE, Josephson ME, Manning WJ, Nezafat R. Scar heterogeneity on cardiovascular magnetic resonance as a predictor of appropriate implantable cardioverter defibrillator therapy. J Cardiov Magn Reson. 2013; 15(1):31.
22. Messroghli DR, Radjenovic A, Kozerke S, Higgins DM, Sivananthan MU, Ridgway JP. Modified Look-Locker inversion recovery (MOLLI) for high-resolution T1 mapping of the heart. Magn Reson Med. 2004; 52(1):141–146. [PubMed: 15236377]
23. Iles L, Pfluger H, Phrommintikul A, Cherayath J, Aksit P, Gupta SN, Kaye DM, Taylor AJ. Evaluation of diffuse myocardial fibrosis in heart failure with cardiac magnetic resonance contrast-enhanced T1 mapping. J Am Coll Cardiol. 2008; 52(19):1574–1580. [PubMed: 19007595]
24. Messroghli DR, Walters K, Plein S, Sparrow P, Friedrich MG, Ridgway JP, Sivananthan MU. Myocardial T1 mapping: Application to patients with acute and chronic myocardial infarction. Magn Reson Med. 2007; 58(1):34–40. [PubMed: 17659622]
25. Weingärtner S, Akçakaya M, Basha T, Kissinger KV, Goddu B, Berg S, Manning WJ, Nezafat R. Combined saturation/inversion recovery sequences for improved evaluation of scar and diffuse fibrosis in patients with arrhythmia or heart rate variability. Magn Reson Med. 2013 [Epub ahead of print].
26. Akcakaya M, Basha TA, Chan RH, Rayatzadeh H, Kissinger KV, Goddu B, Goepfert LA, Manning WJ, Nezafat R. Accelerated contrast-enhanced whole-heart coronary MRI using low-dimensional-structure self-learning and thresholding. Magn Reson Med. 2012; 67(5):1434–1443. [PubMed: 22392654]
27. Lustig M, Donoho D, Pauly JM. Sparse MRI: The application of compressed sensing for rapid MR imaging. Magn Reson Med. 2007; 58(6):1182–1195. [PubMed: 17969013]
28. Block KT, Uecker M, Frahm J. Undersampled radial MRI with multiple coils. Iterative image reconstruction using a total variation constraint. Magn Reson Med. 2007; 57(6):1086–1098. [PubMed: 17534903]
29. Xue H, Greiser A, Zuehlsdorff S, Jolly MP, Guehring J, Arai AE, Kellman P. Phase-sensitive inversion recovery for myocardial T1 mapping with motion correction and parametric fitting. Magn Reson Med. 2013; 69(5):1408–1420. [PubMed: 22736380]

30. Xue H, Shah S, Greiser A, Guetter C, Littmann A, Jolly MP, Arai AE, Zuehlsdorff S, Guehring J, Kellman P. Motion correction for myocardial T1 mapping using image registration with synthetic image estimation. Magn Reson Med. 2012; 67(6):1644–1655. [PubMed: 22135227]
31. Stehning C, Nezafat R, Gharib AM, Desai MY, Weiss RG, Pettigrew RI, McVeigh ER, Stuber M. Dual navigators for time-resolved MR coronary blood flow imaging at 3T during free breathing. Proc Intl Soc Mag Reson Med. 2005:1616.
32. Peters DC, Nezafat R, Stehning C, Eggers H, Manning WJ. 2D cardiac function during free-breathing with navigators. Proc Intl Soc Mag Reson Med. 2007:3860.
33. Akçakaya M, Basha TA, Goddu B, Goepfert LA, Kissinger KV, Tarokh V, Manning WJ, Nezafat R. Low-dimensional-structure self-learning and thresholding: Regularization beyond compressed sensing for MRI Reconstruction. Magn Reson Med. 2011; 66(3):756–767. [PubMed: 21465542]
34. Akçakaya M, Rayatzadeh H, Basha TA, Hong SN, Chan RH, Kissinger KV, Hauser TH, Josephson ME, Manning WJ, Nezafat R. Accelerated late gadolinium enhancement cardiac MR imaging with isotropic spatial resolution using compressed sensing: initial experience. Radiology. 2012; 264(3):691–699. [PubMed: 22820734]
35. Kellman P, Hansen MS. T1-mapping in the heart: accuracy and precision. J Cardiovasc Magn Reson. 2014; 16(1):2. [PubMed: 24387626]
36. Coniglio A, Di Renzi P, Vilches Freixas G, Della Longa G, Santarelli A, Capparella R, Nardiello B, Loiudice C, Bianchi S, D'Arienzo M, Begnozzi L. Multiple 3D inversion recovery imaging for volume T1 mapping of the heart. Magn Reson Med. 2012; 69(1):163–170. [PubMed: 22488966]
37. Warntjes M, Kihlberg J, Engvall J. Rapid T1 quantification based on 3D phase sensitive inversion recovery. BMC Med Imaging. 2010; 10(1):19. [PubMed: 20716333]
38. Akcakaya M, Weingartner S, Roujol S, Nezafat R. On the selection of sampling points for myocardial T1 mapping. Magn Reson Med. 2014 [Epub ahead of print].
39. Chow K, Flewitt JA, Green JD, Pagano JJ, Friedrich MG, Thompson RB. Saturation recovery single-shot acquisition (SASHA) for myocardial T1 mapping. Magn Reson Med. 2014; 71(6): 2082–2095. [PubMed: 23881866]
40. Piechnik SK, Ferreira VM, Dall'Armellina E, Cochlin LE, Greiser A, Neubauer S, Robson MD. Shortened Modified Look-Locker Inversion recovery (ShMOLLI) for clinical myocardial T1-mapping at 1.5 and 3 T within a 9 heartbeat breathhold. J Cardiovasc Magn Reson. 2010; 12:69. [PubMed: 21092095]
41. Higgins DM, Ridgway JP, Radjenovic A, Sivananthan UM, Smith MA. T1 measurement using a short acquisition period for quantitative cardiac applications. Med Phys. 2005; 32(6):1738–1746. [PubMed: 16013731]

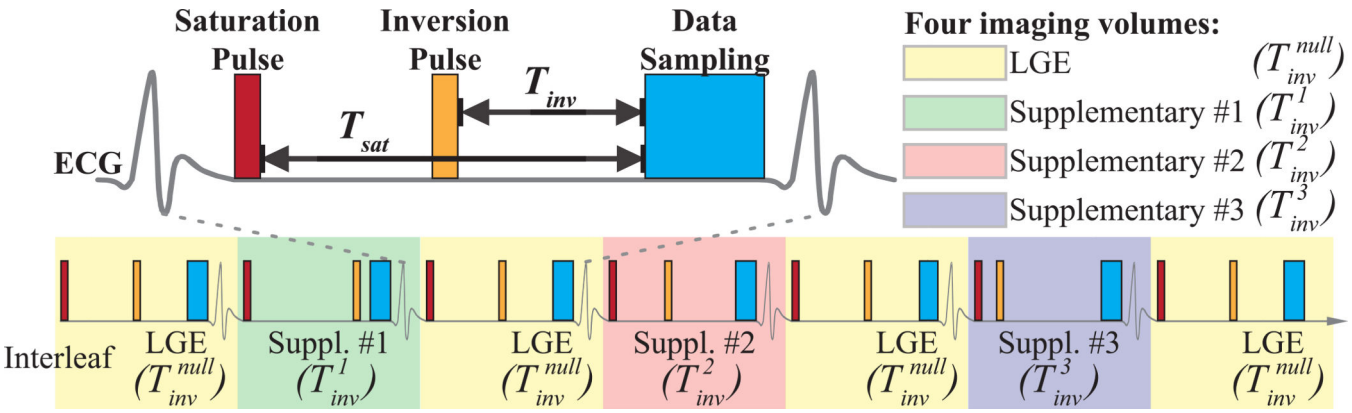

Figure 1. 3D sequence for combined phase-sensitive LGE imaging and T_1 mapping

Four sets of 3D imaging volumes are acquired using hybrid saturation and inversion pre-pulses with different inversion times (T_{inv}^{null}, T_{inv}^{1}, T_{inv}^{2}, and T_{inv}^{3}). Imaging data acquired with T_{inv}^{null} will be used for reconstruction of the 3D LGE image therefore the T_{inv}^{null} time is selected to null the healthy myocardium. T_{inv}^{1-3} times are spread across the RR-interval and the data acquired with these inversion times in addition to the T_{inv}^{null} will be used for calculation of 3D T_1 maps. To obtain fully-sampled LGE data, we propose to acquire data with T_{inv}^{null} in every other heart-beat and acquiring the T_{inv}^{1-3} data in between. This will result in fully sampled LGE data and 3× undersampling of the supplementary images used for T_1 mapping.

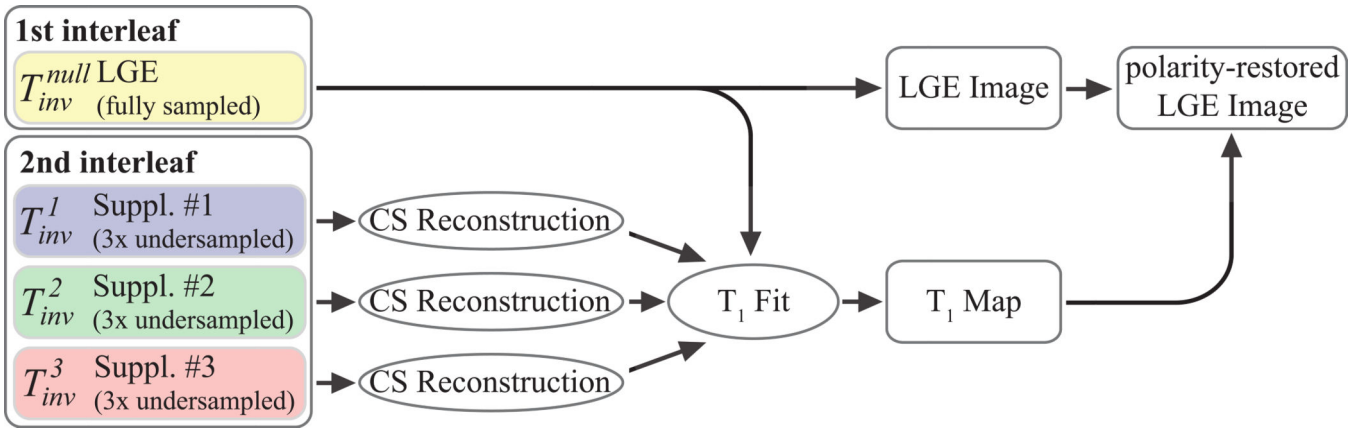

Figure 2. LGE and T_1 Map Reconstruction

3D LGE image is reconstructed by performing a 3D Fast Fourier Transform on the data acquired using the inversion time T_{inv}^{null}. The three remaining datasets corresponding to T_{inv}^{1-3} are first reconstructed using compressed sensing reconstruction. Subsequently, these data and the fully-sampled LGE dataset are used for estimating T_1 maps. Finally, the polarity of the LGE data is restored using the T_1 recovery curve information.

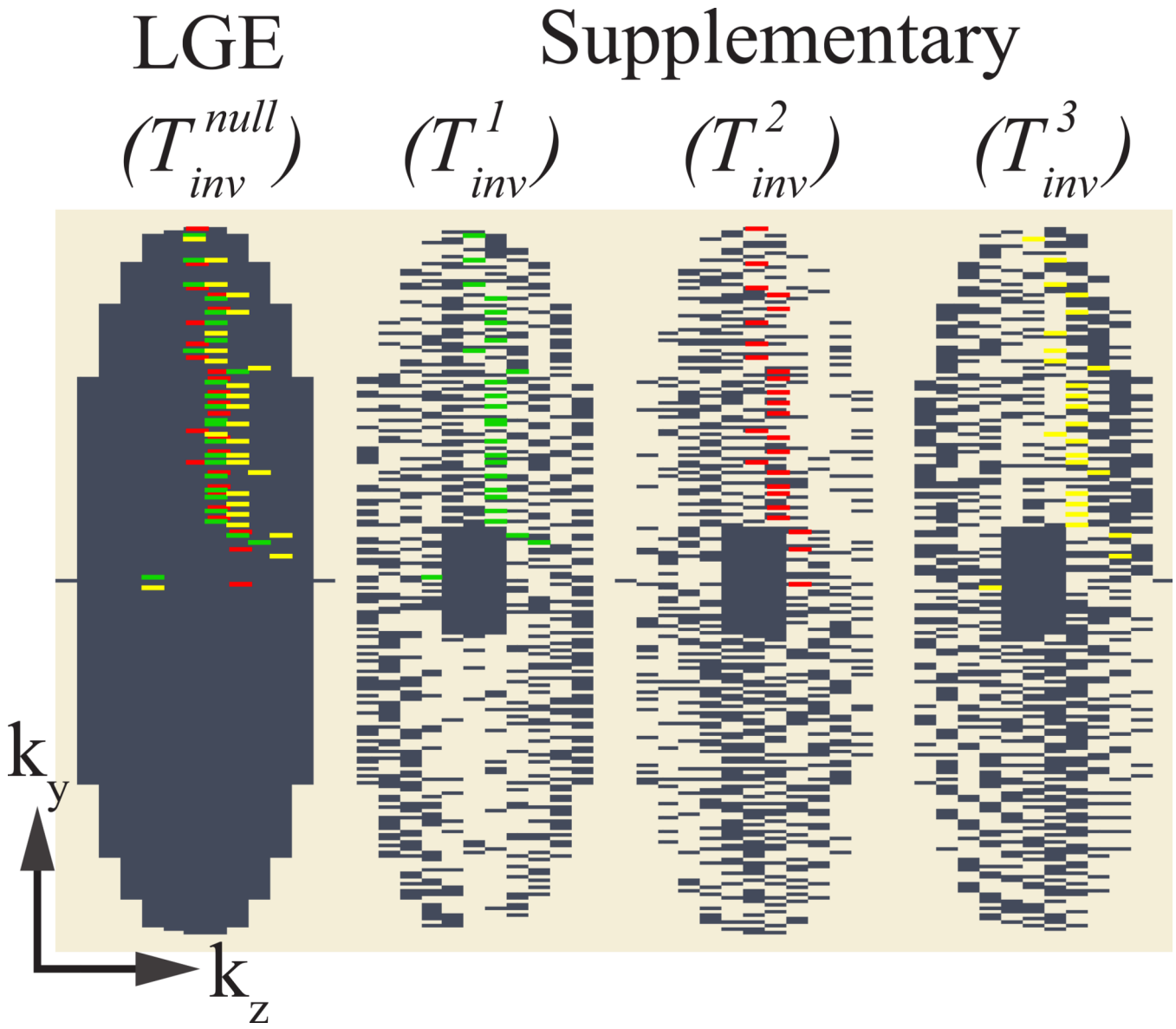

Figure 3. Sampling pattern

Sampling pattern of the fully sampled LGE image and the three three-fold undersampled supplementary images. A k-space shot that is jointly acquired in the first supplementary image and the LGE image is highlighted in green. Similarly k-space shots are highlighted for the second (red) and third (yellow) supplementary image.

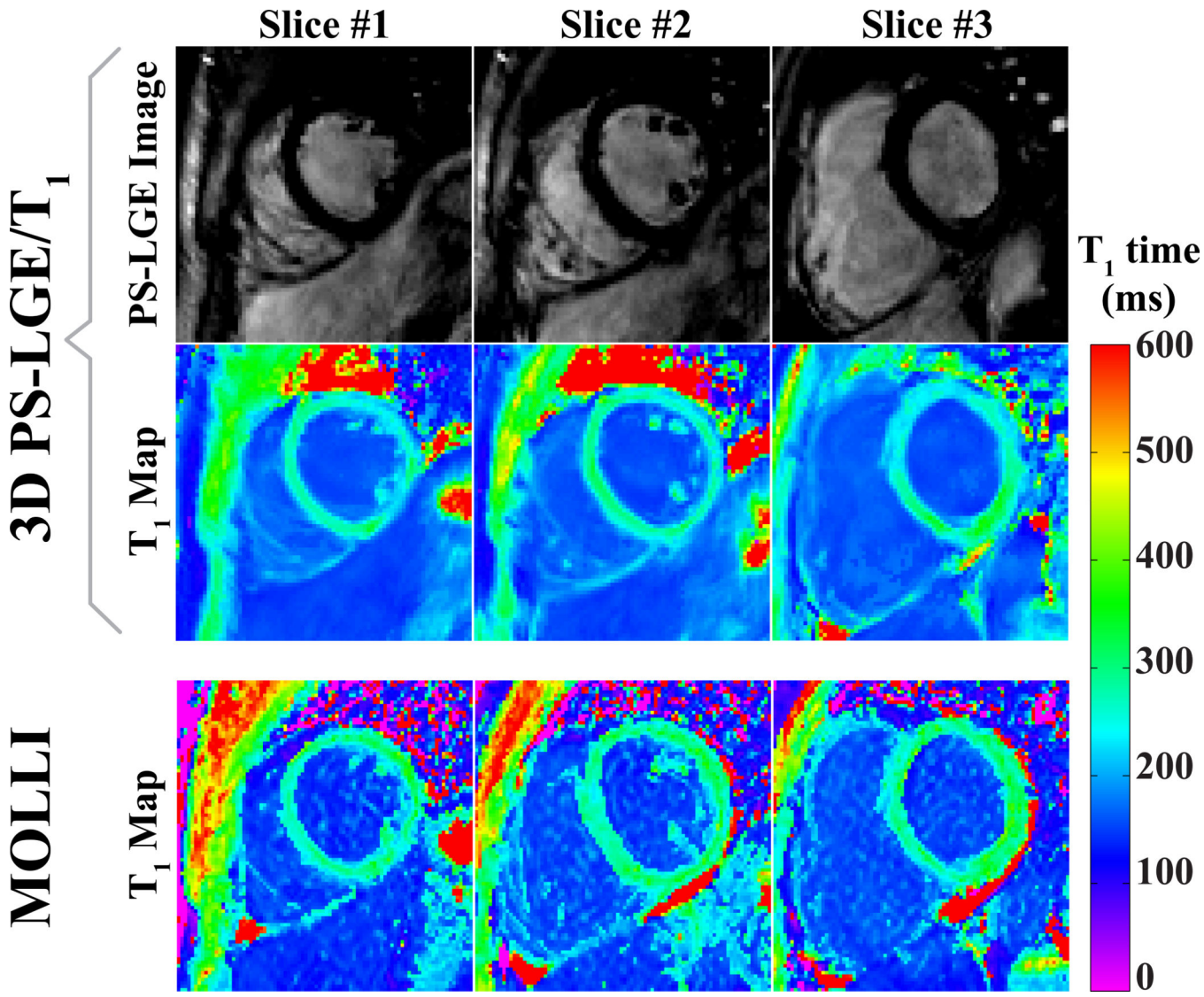

Figure 4.

Combined 3D PS-LGE/T_1 images acquired in a healthy adult subject in comparison to 2D MOLLI T_1. The first and the second row show LGE and T_1 maps reconstructed from the 3D PS-LGE/T_1 sequence. The third row shows corresponding T_1 maps acquired using a 2D multi-slice Modified Look-Locker Inversion Recovery (MOLLI) sequence.

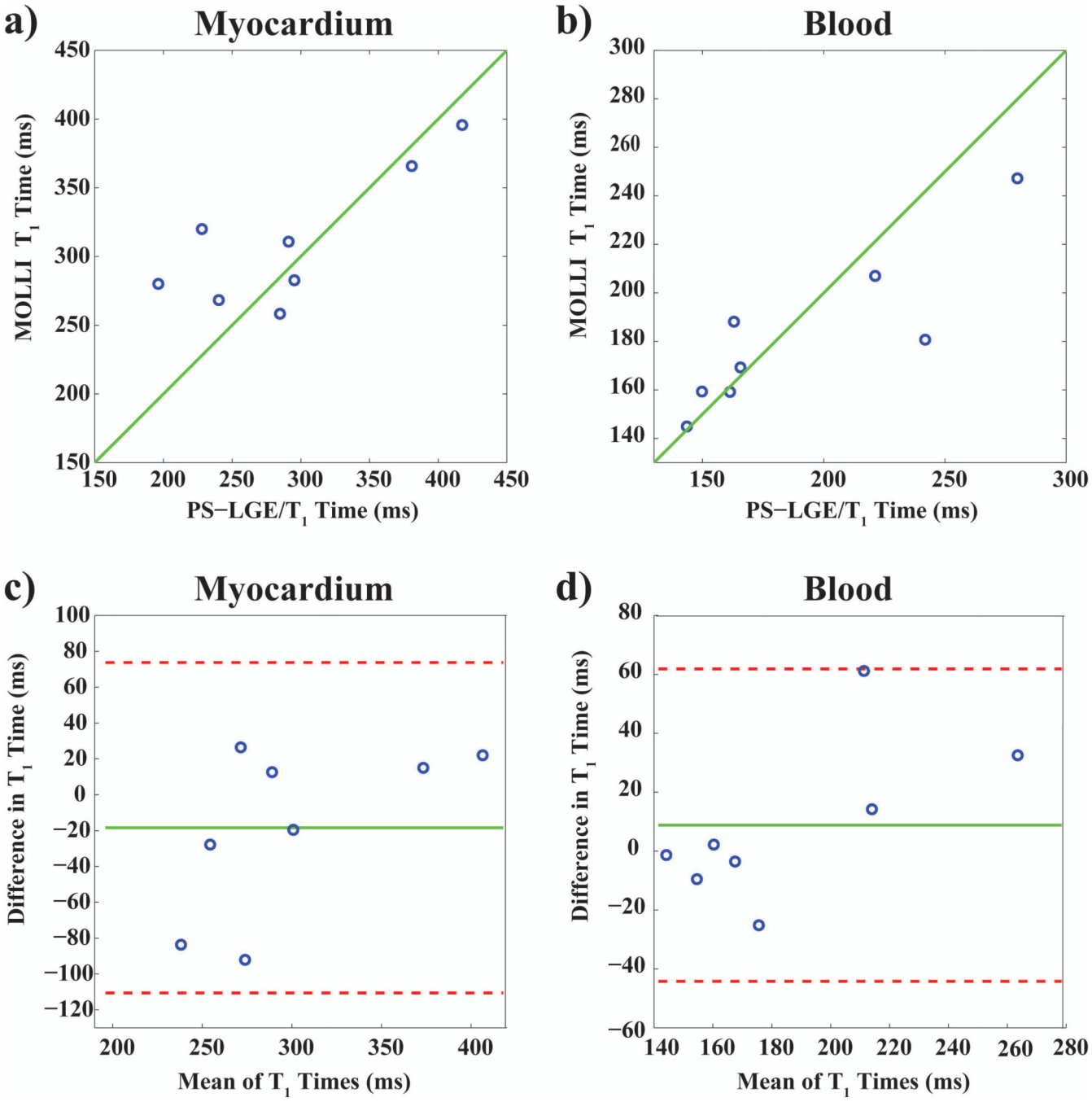

Figure 5.

In vivo T_1 times assessed in the left ventricular (LV) myocardium (left) and the LV and right ventricular (RV) blood pools (right) in eight healthy subjects with the proposed PS-LGE/T_1 sequence and 2D MOLLI. The identity line is indicated in green. The sequences were performed in randomized order. The correlation coefficients were $r = 0.80$ ($p = 0.019$) for the myocardium, and $r = 0.87$ ($p = 0.005$) for the blood. Bland-Altman analysis shows no systematic variations, although more pronounced differences are observed for lower T_1 values.

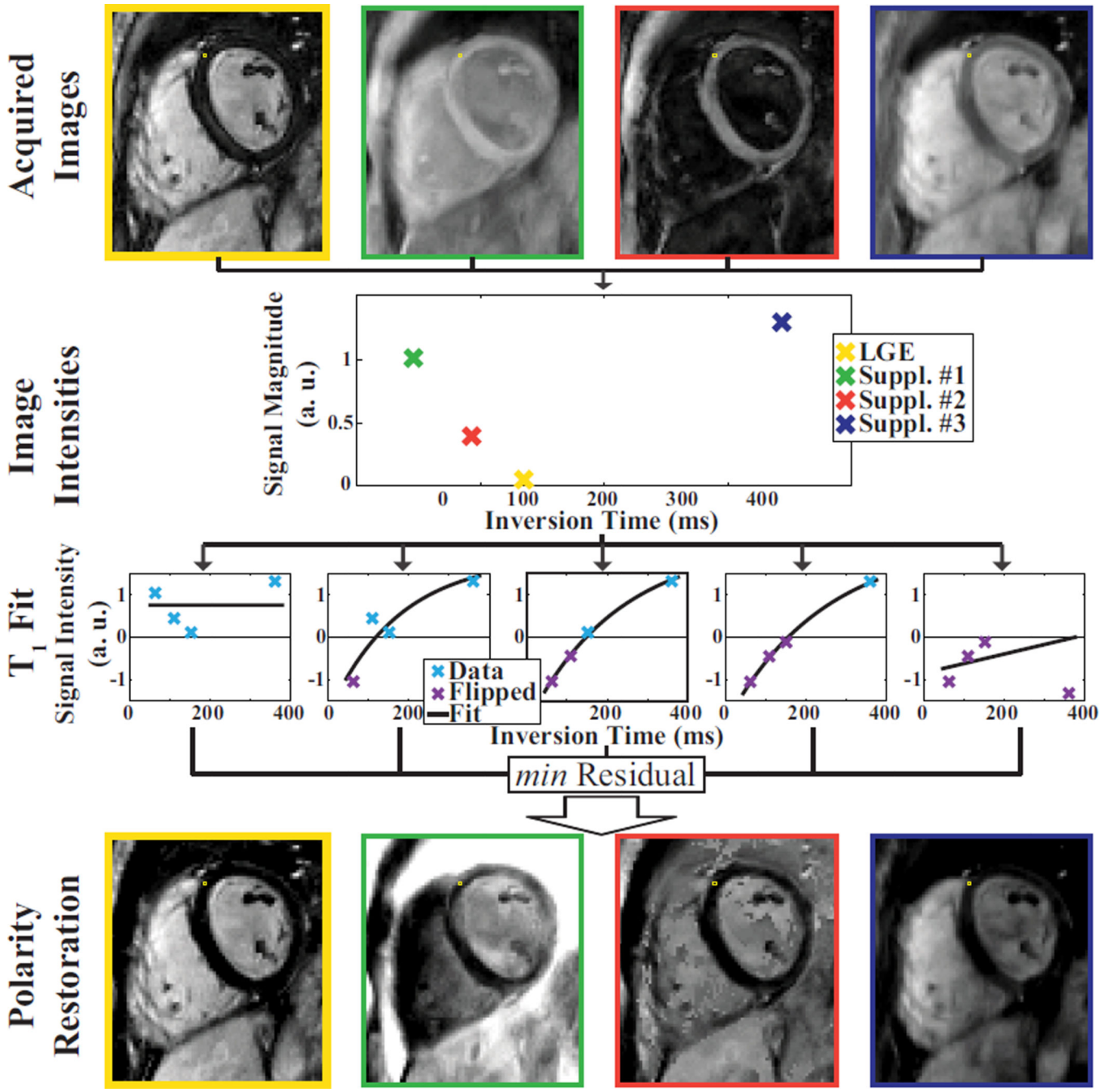

Figure 6.

Scheme for polarity restoration within the T_1 fit process. The upper-most row shows the four acquired imaging volumes after reconstruction. The T_1 fit and the polarity restoration is performed voxel-wise, and illustrated for a sample voxel in this image. The second row shows the intensity magnitude of this voxel in the imaging volume sorted by the inversion time. To restore the signal polarity of the image magnitude the curve-fit to the recovery model is repeated five times, as shown in the third row. The first fit is performed on data where all intensities are assumed to have a positive sign. The second fit is performed under

the assumption that only the data point with the shortest inversion time has a negative sign, and so on. The fitted curve that results in the least residual fit error was assumed to work on the image intensities with corrected polarity. Subsequently, the sign as determined in this multi-fit approach is voxel-wise multiplied with the original intensity magnitude to obtain a polarity-restored LGE imaging volume. The four imaging volumes after polarity restoration are shown in the bottom row. The LGE image after polarity restoration is highlighted by a yellow frame.

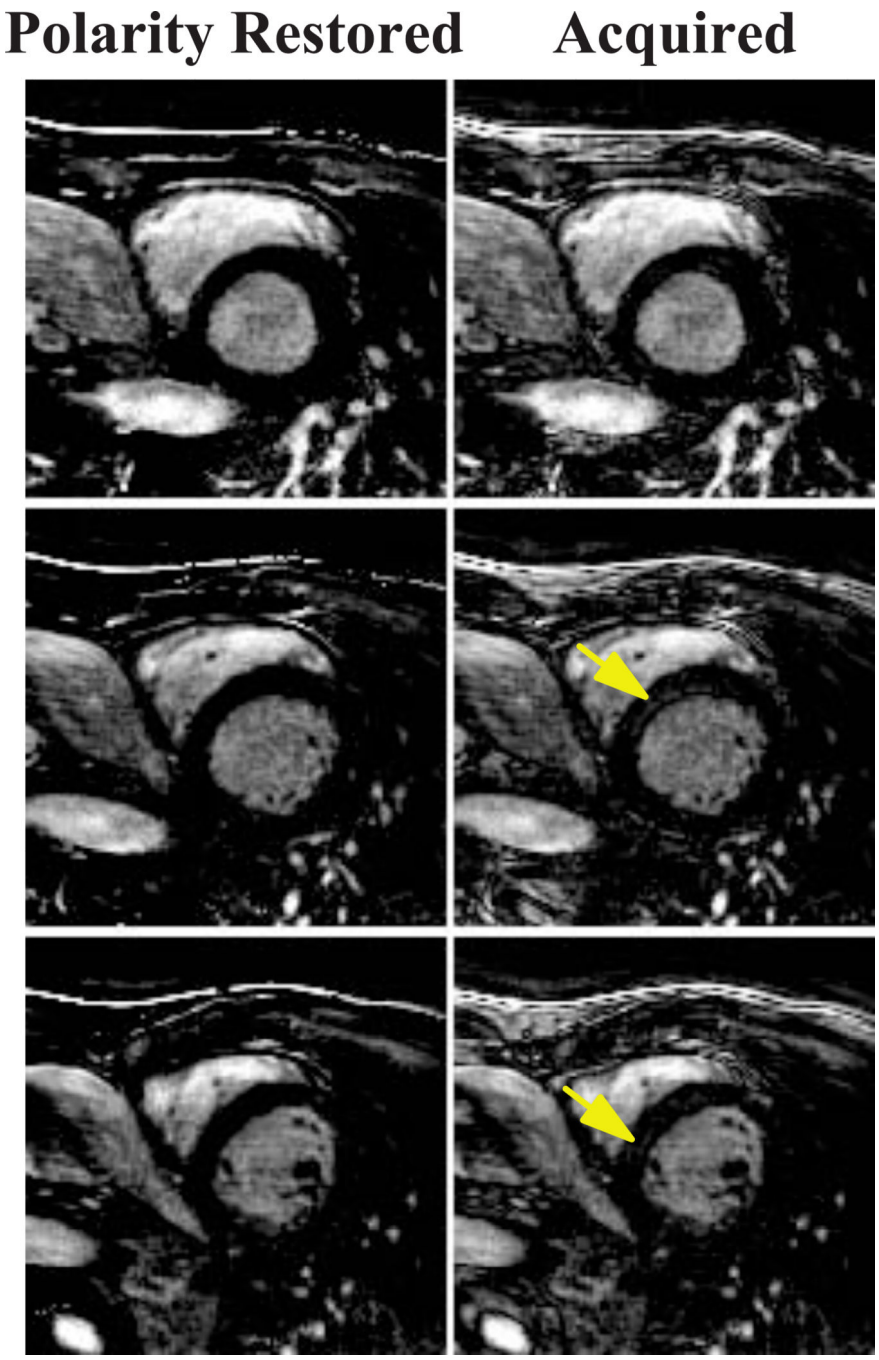

Figure 7.

LGE images acquired in a healthy subject with the proposed 3D PS-LGE/T_1 sequence. Due to an inaccurate inversion-time, artefactual signal enhancement (arrows) can be observed in the LGE image with standard 3D FFT reconstruction. After polarity restoration, the artifact in the myocardium is removed, resulting in complete nulling of the healthy myocardium.

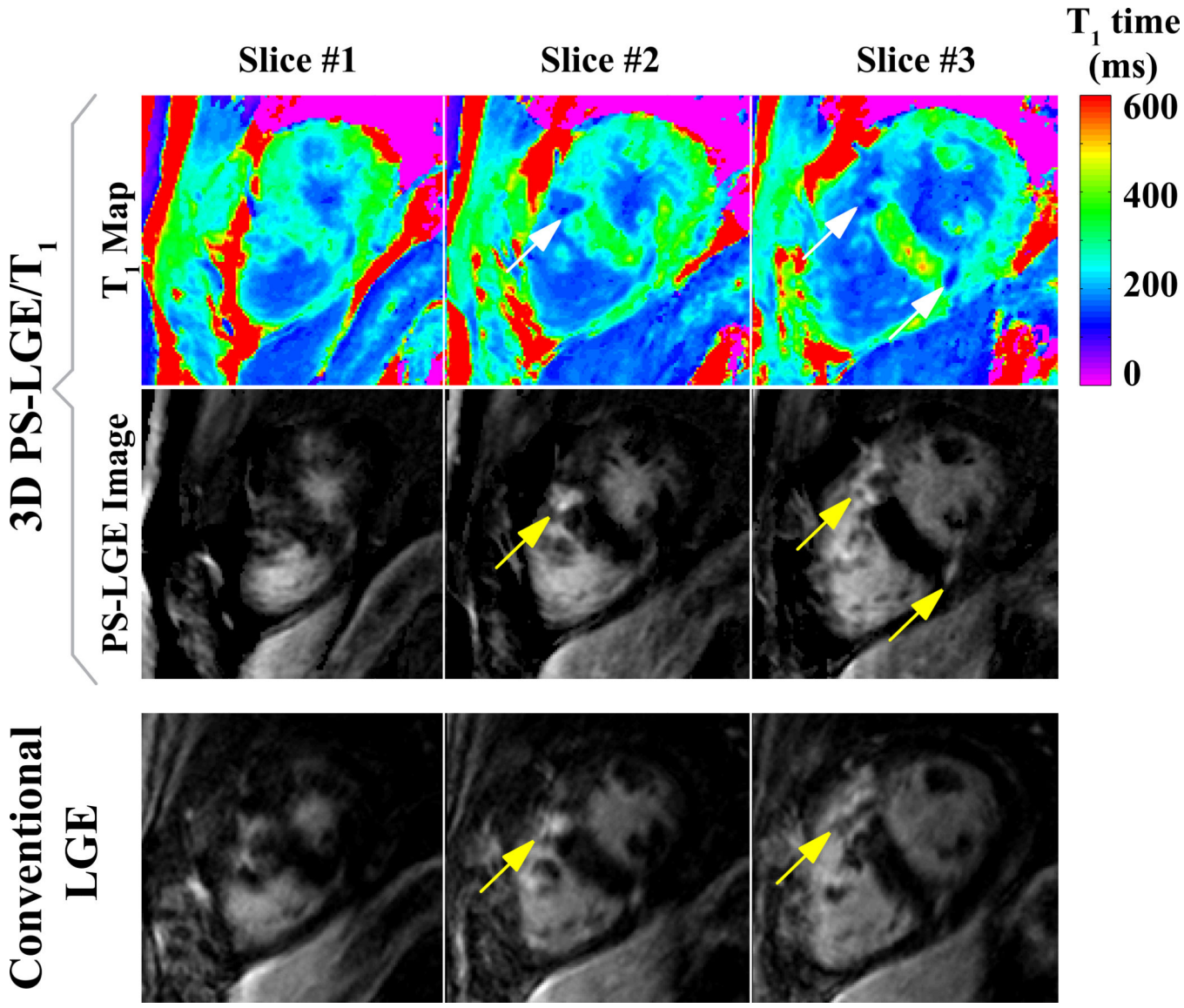

Figure 8.

LGE images and T_1 maps acquired in an HCM patient. Clear depiction of scar at the RV insertion point can be seen in both LGE images and in the T_1 maps (arrows).

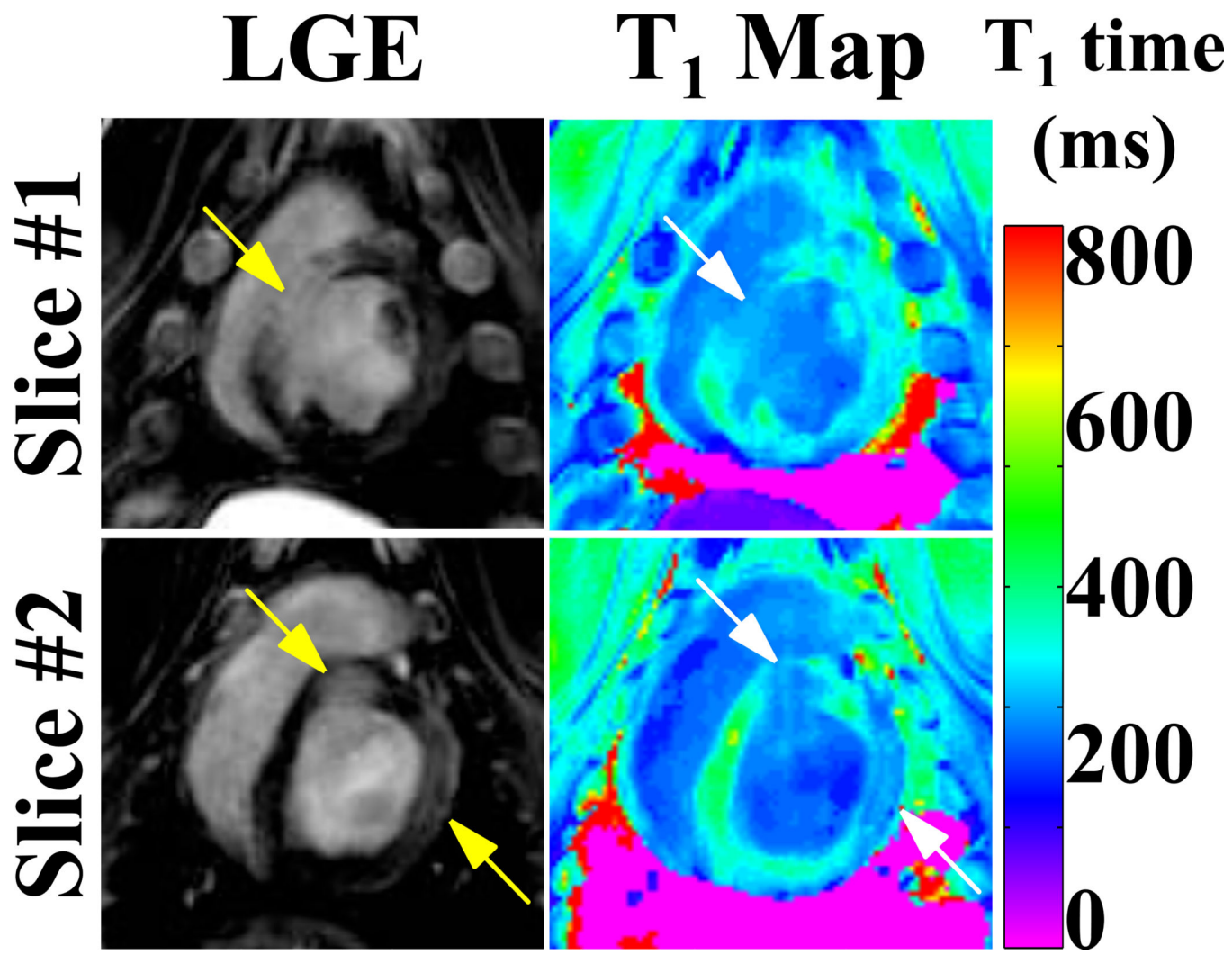

Figure 9.

LGE images and T_1 maps acquired in an animal subject with the proposed sequence, depicting scar in the left ventricle. Clear depiction of the scar and substantially decreased T_1 times in the T_1 maps can be observed (arrows).

Table 1

T_1 accuracy measured in a phantom experiment using the proposed LGE/T_1 sequence, defined as the absolute difference of the mean T1 time in each vial and the spin-echo reference, averaged over ten repetitions. The proposed sequence was performed with different inversion-times in the LGE image, resulting in nulling of the different vials. Each sequence was repeated 10 times. The reference T_1 times, assessed with an inversion recovery spin-echo sequence are given in parentheses.

	Accuracy			
LGE/T_1	**Vial #1 (271 ms)**	**Vial #2 (327 ms)**	**Vial #3 (420 ms)**	**Vial #4 (583 ms)**
nulling: Vial #1	2.7	5.6	2.8	9.4
nulling: Vial #2	2.6	5.9	3.1	9.2
nulling: Vial #3	1.6	5.3	4.0	9.1
nulling: Vial #4	2.9	6.3	4.2	10.4